



# Determination of low-level temperature profiles from microwave radiometer observations during rain

Andreas Foth<sup>1</sup>, Moritz Lochmann<sup>1</sup>, Pablo Saavedra Garfias<sup>1</sup>, and Heike Kalesse-Los<sup>1</sup>

<sup>1</sup>Leipzig Institute for Meteorology, Leipzig University, Leipzig, Germany

**Correspondence:** Andreas Foth (andreas.foth@uni-leipzig.de)

**Abstract.** Usually, microwave radiometer observations have to be discarded during rain. The instrument gets wet which hampers accurate measurements since the retrieval algorithms to derive atmospheric quantities are not trained for rain events. The reason for the latter is, that the rain drops dominate the microwave signal compared to the weaker signal from atmospheric gases. To account for this, radiative transfer simulations need to include the electromagnetic properties of rain, which usually requires more complicated and expensive simulations. In this work, the performance of newly developed microwave radiometer retrievals that are not based on rain simulations is evaluated to assess how they work during rain events. It is shown that it is possible to retrieve low-level temperature profiles during rain by omitting certain frequencies and zenith observations. Retrievals with various combinations of elevation angles and frequencies are evaluated. It is presented that, retrievals based on scanning mode observations with angles below 30° without zenith observation and only the lesser transparent upper four HATPRO microwave radiometer frequencies of the V-band (54.94, 56.66, 57.3, 58 GHz) provides the best results. An analysis of the calculated degrees of freedom of the signal shows that the retrieval of temperature profiles up to 3 km for no rain, 2 km for light to moderate rain and 1.5 km for heavy rain is driven by the HATPRO observation and not by climatology. Finally, the performance of the temperature profile retrieval is explained using a case study in Lindenberg, Germany, and evaluated with temperature profiles from European Center for Medium-range Weather Forecasts (ECMWF) model for different rainfall intensities. The results show that the higher the rainfall rate, the larger the deviation of the microwave radiometer temperature profile retrieval result from the reference model output.

## 1 Introduction

The continuous development and improvement of weather and climate models poses a great challenge to atmospheric remote sensing. For the evaluation of the models, increasingly better-resolved measurements and retrieval methods are needed, e.g. regarding air temperature profiles. Conventional remote sensing observational approaches mainly fail as they are incapable to provide continuous observations of temperature profiles under all weather conditions and especially during rain. Ground-based Raman lidars can usually measure temperature and humidity profiles only below clouds and certainly not during rain (Wandinger, 2005). Radiosondes can provide these atmospheric profiles with high vertical resolution, but they are only routinely available at selected locations and at maximum every 6 hours. Additionally, radiosondes show a significant sonde-to-sonde variability (Nash et al., 2005) as well as a dry bias (Turner et al., 2003).



Multifrequency microwave radiometers (MWR) can provide temporally highly resolved profiles of temperature and humidity, as well as integrated water vapor and liquid water path (Solheim et al., 1998; Güldner and Spänkuch, 1999; Westwater et al., 2005; Rose et al., 2005). Valid retrievals are, however, generally only possible during non-raining conditions (Ware et al., 2004). During rain the atmosphere becomes opaque mainly at high frequencies in the microwave region and no information can be retrieved from higher altitudes. Additionally, the instrument gets wet and the received signal is dominated by the liquid water accumulated on the instrument. In previous studies Cimini et al. (2011) and Ware et al. (2013) compared retrieved profiles of temperature and absolute humidity from a neural network approach (scanning and zenith) and a one-dimensional variational (1DVAR) technique under  $15^\circ$  elevation angle with soundings during all weather conditions. For atmospheric profiling from the surface to 10 km, Cimini et al. (2011) obtained retrieval errors within 1.5 K for temperature and  $0.5 \text{ g m}^{-3}$  for absolute humidity. Xu et al. (2014) retrieved thermodynamic profiles such as temperature and humidity as well as liquid water profiles by using off-zenith MWR observations at  $15^\circ$  elevation to reduce the impact of rain on the measurements. As retrieval technique Xu et al. (2014) used a neural network approach. The temperature bias and root mean square error against radiosondes in precipitation were reduced from 3.6 and 4.2 K to 1.3 and 3.1 K, respectively, compared to the zenith MWR observations. Later, Araki et al. (2015) compared the method from Xu et al. (2014) with 1DVAR technique using zenith and off-zenith observation during raining and non-raining conditions. Their results were evaluated with co-located radiosondes. It was shown that the error in retrieved temperature and water vapor profiles in the low-level troposphere can be reduced by the 1DVAR technique even during rainfall with rain rates less than  $1 \text{ mm h}^{-1}$  by using off-zenith observations. In the presented study, the impact of rain is reduced by using elevation scans only of off-zenith measurements, i.e., at lower elevation angles, because liquid water usually accumulates at the top of the MWR. Furthermore, the influence of rain can be reduced by using only the higher frequencies of the oxygen absorption complex (V-band) which are almost saturated and will thus not be influenced so strongly by liquid water. The idea of the method presented here is that you can use the common measurement mode that you use for non-rainy situations anyway. We show that there is no need to constantly change the measurement mode according to the weather conditions.

The structure of the manuscript is as follows: used instruments such as MWR and radiosondes, European Center for Medium-range Weather Forecasts (ECMWF) model, ERA5 model and radiative transfer models are introduced in the Sec. 2 followed by a description of the retrieval methodology (Sec. 3). The retrieval performance based on simulations and observations as well as a comparison of the observations with the ECMWF model output are evaluated in Sec. 4.

## 2 Instrument and Models

Almost all remote sensing data presented in this work were gathered at the Meteorological Observatory Lindenberg - Richard-Assmann-Observatory (MOL-RAO,  $52.208^\circ\text{N}$ ,  $14.118^\circ\text{E}$ ) in Lindenberg, Germany, during an instrument intercomparison campaign from July 16, 2020 until October 10, 2020. In addition to that, MWR data presented in Sec. 3 was gathered at the Leipzig Institute for Meteorology, Leipzig University ( $51.333^\circ\text{N}$ ,  $12.389^\circ\text{E}$ ). The used instruments and models are explained in the following subsections.

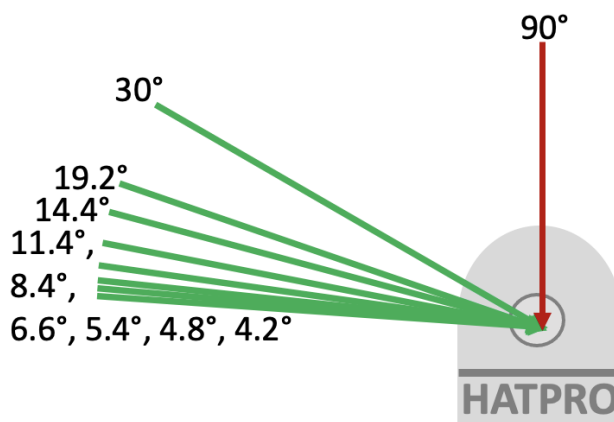


**Figure 1.** HATPRO's default set of elevation angles. Green and red arrows show off-zenith and zenith elevation angles, respectively.

## 2.1 Microwave radiometer HATPRO

The humidity and temperature profiler (HATPRO, generation 5) is a fully automatic microwave radiometer (MWR) from the manufacturer Radiometer Physics GmbH (Rose et al., 2005). It is a passive instrument and measures atmospheric emission at 14 frequencies along the microwave spectrum with a high temporal resolution of 1 s. Seven frequencies are situated along the upper wing of the water vapor absorption band at 22 GHz (Ka-band) and seven at the lower wing of the oxygen absorption complex at 58 GHz (V-band). For both absorption bands, HATPRO has its own antenna, which measures voltages of the individual frequencies. The voltages are then calibrated to brightness temperatures by automated calibrations (Kazama et al., 1999; Maschwitz et al., 2013; Kuchler et al., 2016). The antennae are situated below a radome sheet, which is transparent in the microwave region. HATPRO utilizes a rain mitigation system which blows a constant strong air stream over the radome. Nevertheless, during heavy or prolonged rainfall, liquid water might still accumulate on the radome's top, especially if the radome has aged, as is the case during long-term use in the field. This usually prevents the accurate determination of atmospheric variables.

In order to estimate column-integrated variables such as the integrated water vapor and liquid water path, as well as vertical profiles of temperature and humidity, so-called retrievals must be created (Löhnert and Crewell, 2003). Retrievals are based on artificial neural networks or multi-linear regression models which are trained on relations between measured brightness temperatures and the wanted quantity from radiosondes or numerical weather prediction model output. Observations under different elevation angles enhance the accuracy of the retrieved temperature profile within the atmospheric boundary layer (Crewell and Löhnert, 2007). A sketch showing the HATPRO's measurements at default elevation angles color-coded by zenith and off-zenith is illustrated in Fig. 1. Those angles were intentionally selected to represent 1, 2, 3, 4, 5, 7, 9, 11, 12, and 14 air masses.



## 2.2 Radiosondes

Radiosondes provide highly resolved vertical information of atmospheric temperature, humidity and pressure. Here we used  
80 a large data set of 9555 Vaisala RS80 soundings from June 1996 to November 2003. This serves as input into radiative transfer  
calculations to create the synthetic brightness temperatures used for the retrieval algorithm to estimate temperature profiles (see  
Sec. 2.5). Their accuracy in contrast to other types of radiosondes is described by Turner et al. (2003). For the comparisons  
of temperature profiles in Sec. 4.2, Vaisala RS41 radiosondes are used (Sun et al., 2019; Jensen et al., 2016). In the presented  
work, all radiosondes were launched at MOL-RAO.

## 85 2.3 European Center for Medium-range Weather Forecasts model

In this study, temperature profiles from ECMWF Integrated Forecast System (IFS) are used to evaluate the retrieved temperature  
profiles from the MWR observations. This is done because the ECMWF-IFS model data is available in a higher temporal  
resolution (hourly) than that of the radiosondes. The model data used here are stored in the Cloudnet categorization product  
(Illingworth et al., 2007) which is freely available at <https://cloudnet.fmi.fi/search/data?site=lindenberg> (last access, 27 Mar,  
90 2024).

## 2.4 ERA5

ERA5 (ECMWF Reanalysis v5) is the fifth generation of ECMWF's atmospheric reanalysis of global climate. ERA5 is pro-  
duced by the Copernicus Climate Change Service (C3S) at ECMWF and covers data from 1940 to present. Here, hourly profiles  
of temperature, humidity and pressure with a vertical resolution of 137 pressure levels from the surface up to a height of 80 km  
95 are extracted from the global data-set for the MOL-RAO site. 58195 profiles from the ERA5 data set from 2000 to 2019 are  
used as input for the radiative transfer calculation for the temperature retrieval creation.

## 2.5 Non-scattering microwave radiative transfer model

Based on Simmer (1994), the non-scattering microwave radiative transfer is applied to calculate the brightness temperatures of  
each profile from 9555 radio-soundings and 58195 ERA5 profiles. This results in a data-set of 67750 profiles with correspond-  
100 ing calculated brightness temperatures which serve as base for the retrieval generation. It uses the gas absorption by Rosenkranz  
(1998) and liquid water absorption by Liebe (Liebe et al., 1993). The Rosenkranz gas absorption model is corrected for the  
water vapor continuum absorption according to Turner et al. (2009). Uncertainty of atmospheric microwave absorption models  
and their impact on ground-based radiometer simulations and retrievals are extensively described in Cimini et al. (2018). The  
model code is written in the interactive data language (idl) and was ,e.g. also applied in Löhnert and Crewell (2003); Löhnert  
105 et al. (2007); Foth and Pospichal (2017).



## 2.6 Passive and Active Microwave TRAnsfer PAMTRA

The Passive and Active Microwave TRAnsfer tool (PAMTRA) solves the radiative transfer for passive and active microwave radiation in all-sky conditions, i.e. cloudless, cloudy, and precipitating atmospheres (Mech et al., 2020). In this study, PAMTRA is used to simulate the brightness temperatures at the HATPRO frequencies during rain to investigate the impact of rain in the atmosphere and to assess liquid water accumulation on the radome (see Sec. 3.2).

## 3 Methodology

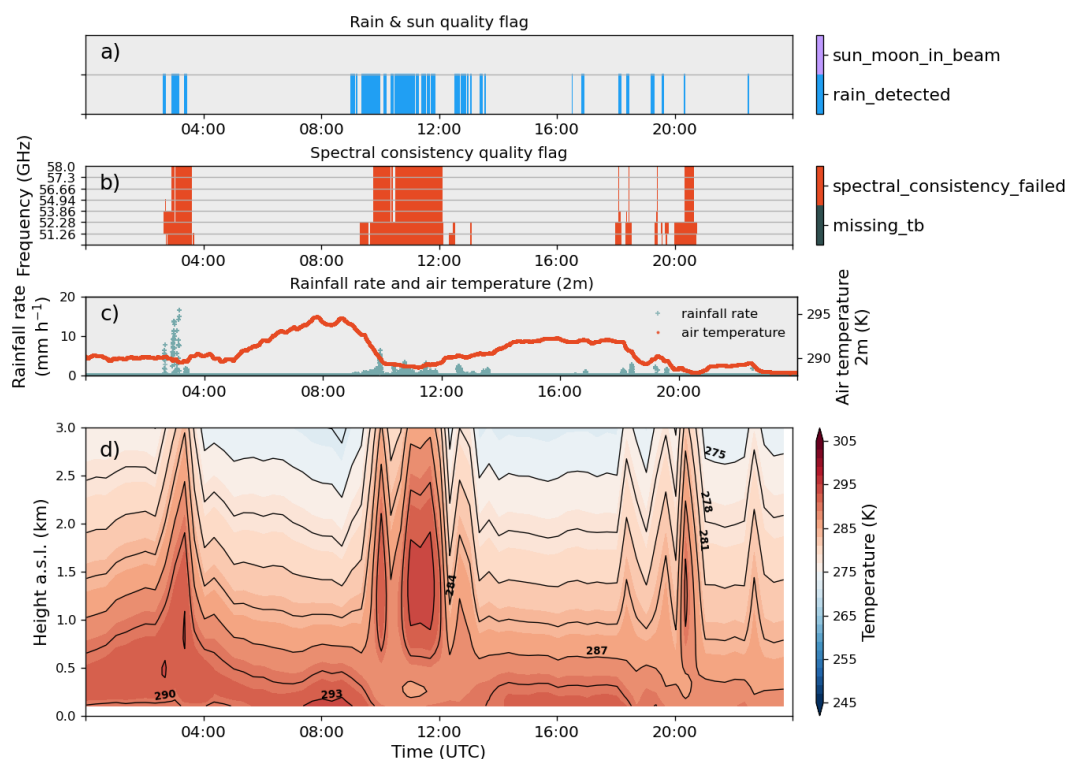
In this section, the problem of retrieving temperature profiles during rain is first shown using an example. Then the theoretical basics of how to create a temperature retrieval are explained. Finally, the procedure to select the most relevant frequencies and elevation angles is explained and the results of the information content analysis are shown. Figure 2 (d) illustrates the problem of state-of-the-art temperature retrievals during rain, indicated by unrealistic spikes. The rain and sun quality flag (a) denotes if rain was detected by HATPRO's weather station or if the Sun or the Moon is directly in the receiver's field of view. Both would affect the quality of the retrieval. The second panel (b) shows the results of the spectral consistency check which is retrieved by the so-called *tbx* retrievals, which work as follows. There are 14 HATPRO frequencies and only 13 of them are used to estimate the expected value for the 14th frequency and then the difference between the estimated and the measured brightness temperature is determined. This procedure is repeated for all 14 frequencies. If the brightness temperature difference at a given frequency exceeds the limits of 1 K for Ka-band and 2 K for V-band, the time steps are flagged with *spectral consistency failed*. This usually happens when nonphysical or unrealistic spectra are measured due to rain or other obstacles in the field of view. During rainy periods none of the frequencies has passed the consistency check, therefore none of the frequencies are reliable to be used. Thus, the state-of-the-art retrieval will not be trustworthy.

Figure 2 (c) shows the temperature variation and rainfall rate from the HATPRO weather station during the day. There are obviously no major temperature gradients during rain events that might explain the height-time series of temperature (d). The presented temperature profiles are retrieved by the RPG firmware retrieval which is based on a neural network approach using all 7 V-band frequencies and all 10 elevation angles. This frequency and elevation angle setup corresponds to the state of the art in determining temperature profiles under rain-free conditions.

All MWR retrievals, including *tbx* retrievals and for temperature profiles, need to be created for each specific geographic region, as typical atmospheric profiles of temperature and humidity vary across the globe. Walbröl et al. (2022) e.g. created MWR retrievals for low-humidity conditions in the Arctic and Schnitt et al. (2024) for the tropical Atlantic.

### 3.1 Temperature profile retrieval method

The retrieval essentially consists of a series of coefficients that can be based on an artificial neural network or a multi-linear regression model that relates modeled brightness temperatures and temperature profiles (Löhnert and Maier, 2012). In this work we use a regression model. The temperature profiles are based on 9555 radiosondes and 58195 ERA5 output profiles



**Figure 2.** Time series of Moon or Sun and rain quality flag (a), spectral consistency quality flag (b), air temperature and rainfall rate from HATPRO's weather station (c), and height-time series of temperature profiles based HATPRO's firmware radiometer retrieval algorithms in Lindenberg (Germany) on Aug 26, 2020. tb in the colorbar (b) means brightness temperature.

corresponding to the location of the MOL-RAO site in Lindenberg. We decided to use these two different data sources to get a data-set which contains profiles with high vertical resolution (radiosonde) and a large amount of profiles with modeled liquid water information (ERA5). From this data-set, temperature, humidity and pressure profiles are extracted. The cloud liquid water content is directly extracted from the ERA5 data. For the radiosonde data a cloud is synthetically determined where 95 % relative humidity is reached (Decker et al., 1978). The modified adiabatic liquid water content is then determined for the altitude range of the cloud according to Karstens et al. (1994). This information is used as input to the non-scattering microwave radiative transfer model (see Sec.2.5). For each input profile the brightness temperatures which would be measured by a microwave radiometer under the given input conditions, frequencies and elevation angles are simulated. In total 54200 profiles (80% randomly chosen profiles) were used for the training and 13550 (20%) to test the regression model to predict the temperature profiles based on simulated brightness temperatures. In this study, different retrieval settings (varying number of frequencies and angles) were generated to contrast the RPG firmware method based on seven frequencies in the V-band



**Table 1.** Retrieval specification. Zenith mode frequencies indicate the frequencies ( $\nu$ ) that are observing only in zenith direction whereas scanning mode frequencies mark those measuring in the directions given by the elevation angle ( $\varphi$ ) in the last column. Retrieval name nomenclature:  $X\nu[z]Y\varphi$ .  $X$ : number of frequencies with elevation scanning;  $Y$ : number of elevation angles. The index  $z$  indicates that, additionally, three zenith observations for 51.26-53.86 GHz have been included in retrieval development (first row). Nomenclature according to Crewell and Löhnert (2007).

	zenith mode frequencies (GHz)	scanning mode frequencies (GHz)	elevation angles ( $^{\circ}$ )
$4\nu z 10\varphi$	51.26, 52.28, 53.86	54.94, 56.66, 57.3, 58	90, 30, 19.2, 14.4, 11.4 8.4, 6.6, 5.4, 4.8, 4.2
$4\nu 10\varphi$	–	54.94, 56.66, 57.3, 58	90, 30, 19.2, 14.4, 11.4 8.4, 6.6, 5.4, 4.8, 4.2
$7\nu 9\varphi$	–	51.26, 52.28, 53.86 54.94, 56.66, 57.3, 58	30, 19.2, 14.4, 11.4 8.4, 6.6, 5.4, 4.8, 4.2
$4\nu 9\varphi$	–	54.94, 56.66, 57.3, 58	30, 19.2, 14.4, 11.4 8.4, 6.6, 5.4, 4.8, 4.2

(oxygen complex) and ten elevation angles including the zenith direction ( $90^{\circ}$ ). Specifically, here a set of 4 retrieval setups are proposed that are only based on the upper four HATPRO frequencies in the V-band which exclude the zenith observation  
 150 (nine angles). The different retrieval setups are listed in Tab. 1. The  $4\nu z 10\varphi$  retrieval is the most commonly used retrieval for low-level temperature profiling during non-rainy conditions. It uses 10 elevation angles (including the zenith angle) and the upper four frequencies of the V-band. Additionally, the lower three frequencies of the V-band are used at the zenith angle.

The question how the frequencies and elevation angles for the new temperature retrievals are selected is discussed in the following subsection. The performance during non-raining (cloudy and cloudless ) conditions is treated in Sec. 4.1 and is  
 155 illustrated in Fig. 5.

### 3.2 Selection of frequencies and elevation angles

To select frequencies and elevations angles for a new temperature retrieval that is less compromised by rain, it is necessary to check which frequencies are less affected by rain accumulated on the radome and by rain in the atmosphere. This was done by a special MWR measurement strategy during a rain event described below. It is worth noting again, that during rain, the  
 160 atmosphere becomes more opaque with increasing frequency in the V-band.

On August 1, 2023, on the roof measurement platform of the Institute for Meteorology of Leipzig University, a special measurement was performed with the microwave radiometer HATPRO. It rained almost continuously from midnight to 8:30 UTC. Rain rates were generally below  $2 \text{ mm h}^{-1}$  but occasionally reached  $7 \text{ mm h}^{-1}$ . Afterwards, there were repeated rain showers and cloudless periods into the night. A scan pattern from  $0^{\circ}$  (horizontal) to  $90^{\circ}$  (zenith) with  $5^{\circ}$  elevation angle steps was  
 165 carried out continuously. In addition, PAMTRA simulations of brightness temperatures at all specified elevation angles were



carried out for three different situations on that day: no rain, moderate rain ( $2.7 \text{ mm h}^{-1}$ ) and heavy rain ( $3.7 - 11 \text{ mm h}^{-1}$ ). The ECMWF model output profiles of temperature, pressure and relative humidity in Leipzig from the same day were taken as input for the simulations. Rain drop size distributions for the stratiform rain event early in the day and a heavy rain shower around 14:14 UTC were measured by a disdrometer (Type: precipitation laser monitor, LNM from Thies; Fehlmann et al. (2020)). The spatial variability of rain drop number concentration in the convective afternoon shower needs to be taken into consideration since during elevation scans low and high angles point towards different atmospheric volumes. For that purpose, PAMTRA simulations were run with a) the original rain drop number concentration observed by the LNM, b) a rain drop number concentration which is only 33 % of a), and c) a rain drop number concentration which is only 66 % of a) and decreases by half with altitude (from surface up to 2.5 km). This variation in the LNM input allows to account for the heterogeneity of rain drop number concentration during convective rain and hence helps to assess differences between observation and simulation. This is important since PAMTRA assumes horizontally homogenous conditions.

The brightness temperatures difference between HATPRO observations and PAMTRA simulations as a function of the elevation angle are illustrated in Fig. 3 (a, b, c) for the seven frequencies in the V-band and for three weather conditions. It can be seen that the simulation and observation fit well for the profile with no rain at 14:33 UTC. The differences originate in the simulation which might be caused by the ECMWF model input which slightly differs from the atmospheric state that was observed by MWR. For the profile at 7:41 UTC with rain rates around  $2.7 \text{ mm h}^{-1}$  the brightness temperatures from 51.26, 52.28, and 53.86 GHz differ from the simulation above  $70^\circ$  elevation angle. This might be caused by the accumulation of liquid water from rain on the top of the MWR radome. For the heavy rain shower at 14:14 UTC with rain rates between  $3.7 \text{ mm h}^{-1}$  and  $11 \text{ mm h}^{-1}$  the simulated and the observed brightness temperatures at the same three frequencies differ by up to 50 K above  $40^\circ$  elevation angle. 54.94, 56.66, 57.3, and 58 GHz as well as all angles below  $45^\circ$  are apparently unaffected by the impact of rain and show no significant difference between simulated and observed brightness temperatures. That means that all elevation angles below  $40^\circ$  and the upper four HATPRO frequencies from the V-band can be used to retrieve temperature profiles during rain. It is important to note that most state-of-the-art temperature retrievals from boundary layer scans (e.g. HATPRO's firmware) uses the set of elevation angles shown in Fig. 1, thus the majority of elevation angles used by the retrievals are below  $40^\circ$  except for the zenith observation.

One might expect that the addition of the lower HATPRO frequencies of the V-band (i.e. using all seven frequencies in the retrieval) would be more suitable, as the atmosphere is more transparent at these frequencies. This might be the case if the algorithm pursues to additionally retrieve rain parameters, however for this work we are interested in retrieving only temperature profiles and our analysis have shown that for that purpose the lower V-band frequencies are not optimal and instead increase uncertainties. Horizontally homogeneous conditions are assumed for boundary layer scans. At low elevation angles, however, different air masses are observed by the less and more transparent channels leading to uncertainties in the retrieved profiles.



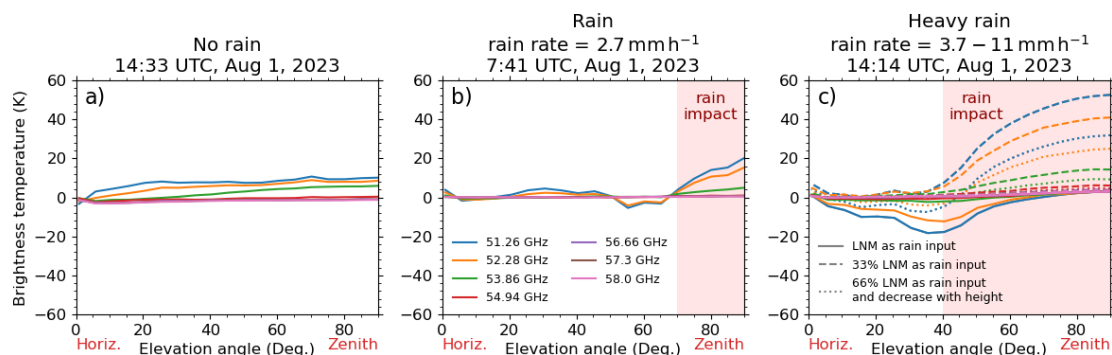


**Figure 3.** Difference between observed and simulated brightness temperatures for different frequencies (colors) versus elevation angle for no rain (a), rain (b), and heavy rain events (c). Different line styles in (c) label different LNM rain inputs into the PAMTRA simulation. Rose rectangle marks the area where the observations significantly differ from the simulation probably caused by wet radome.

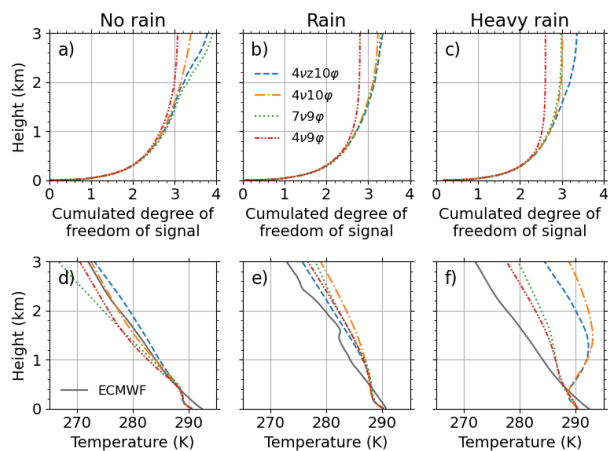


**Figure 4.** The cumulated degrees of freedom of signal and temperature profiles for no rain (a, d), rain (b, e) and heavy rain (c, f) conditions on Aug 1, 2023.



### 3.3 Information content analysis

To investigate how much information originates from the observations and not from the climatology, an optimal estimation  
200 technique has been applied (Rodgers, 2000; Maahn et al., 2020). It calculates the degree of freedom of a signal and gives the  
information content that comes from the measurement itself. The cumulated degree of freedom of signal of all four retrievals  
are illustrated in Fig. 4 for the three conditions (a, b, c) mentioned in Sec. 3.2. The curves of all retrievals have a similar shape  
and differ only slightly in the upper layers. With increasing altitude, the difference of cumulative degrees of freedom of signal  
are larger. Once the curve reaches a vertical line no more information is added by the measurements. The retrievals with fewer  
205 frequencies and angles ( $4\nu_{10\varphi}$ ,  $4\nu_{9\varphi}$ ) display lower values of the cumulated degrees of freedom of signal under all three  
weather conditions. This means that there is less information from altitudes above roughly 1.5 km from the measurement and  
the profile is more driven by the climatology. The more rain there is in the atmosphere, the lower the information content of the  
measurement, as can be seen in the maximum value of the cumulated degree of freedom of signal in 3 km which reaches values  
between 3 and 4 for no rain and between 2.8 and 3.4 during rain and between 2.6 and 3.4 during heavy rain. Summarizing,  
210 the retrieved temperature profile is driven by the measurement at least up to 3 km for no rain, about 2 km for rain and about  
1.5 km for heavy rain proven by the determined degree of freedom of signal indicated by the point at which the line with lowest  
information content (red) becomes vertical.

The retrieved temperature profiles from the four retrievals, as well as the ECMWF temperature output profile for the same  
three conditions (no rain, rain, heavy rain) are illustrated in Fig. 4(d, e, f). As expected for non-rainy conditions (d) and shown  
215 in section 4.1,  $4\nu_{z10\varphi}$  and  $4\nu_{10\varphi}$  show the smallest difference to ECMWF output which serves as reference here. But also the  
 $4\nu_{9\varphi}$  performs similarly. Only the  $7\nu_{9\varphi}$  underestimates the ECMWF temperature in higher altitudes and which may be caused  
by the fact that frequencies with different transparencies observe different air masses at lower elevation angles, as explained  
above. For the rain case (e), all retrievals perform similar although the zenith observation is affected by rain as shown in  
Sec. 3.2, which might indicate that at the observed rain rates of  $< 2.7 \text{ mm h}^{-1}$  temperature retrieval profiles are less affected  
220 by rain in the atmosphere. For the heavy rain event (f), the  $4\nu_{9\varphi}$  retrieval shows the best performance indicated by the smallest  
difference to the reference ECMWF model output. As expected  $4\nu_{z10\varphi}$  and  $4\nu_{10\varphi}$  have largest deviations from ECMWF  
model output since they are intentionally made for non-rainy conditions.

## 4 Results

This section first shows the performance of the newly created temperature profile retrievals based on simulations with the test  
225 data-set under non-rainy conditions. This is only to show that the new different retrievals produce meaningful results. In section  
4.2, the retrieval performance is evaluated on the basis of observations using the case study introduced in Sec. 3. Finally, the  
retrieved temperature profiles are compared to ECMWF output on a larger data-set.

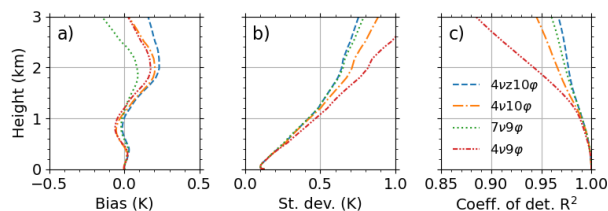


**Figure 5.** Temperature retrieval performance in terms of bias (a), standard deviation (b) and coefficient of determination (c) based on synthetic data (trained with radio-soundings and ERA5) during cloudy and cloudless conditions.

#### 4.1 Retrieval performance based on simulations during non-raining conditions

The performance of the new approaches ( $7\nu10\varphi$ ,  $4\nu10\varphi$ ,  $4\nu9\varphi$ ) in comparison to the common retrieval ( $4\nu z10\varphi$ ) under non-raining idealized conditions is shown in Fig. 5. This is the result of the test data from the atmospheric profiles from radiosonde and ERA5. Bias (a), standard deviation (b), and coefficient of determination (c) between true values and the prediction of the regression model indicate how much uncertainty is added by omitting frequencies and elevation angles during cloudy and cloudless conditions using profiles from the test data-set. All four sets of retrievals show similar behavior in bias (a), namely just small systematic deviations from zero at around 2 km. For all four retrievals, standard deviation (b) increases with altitude while  $R^2$  decreases with altitude, both indicating an increase in uncertainty with height. Bias, standard deviation and  $R^2$  values are in accordance with Crewell and Löhnert (2007). Highest uncertainties are evident for the  $4\nu9\varphi$  retrieval. This is an expected behavior since information can be lost by omitting frequencies and zenith observations as shown in Fig. 4, whereas the  $4\nu9\varphi$  retrieval was optimized for rainy conditions.

#### 4.2 Case study based on observations

If the four versions of the temperature retrieval (Tab. 1) from the previous section are applied to the MOL-RAO example on Aug 26, 2020, from the problem description (Sec. 2), one can see the improvement by selecting only lower elevation angles and the higher frequencies. Figure 6 shows the height-time plots of the four temperature retrievals (b, d, f, h), the ECMWF model temperature (a), as well as the difference to the ECMWF model temperature (c, e, g, i). As introduced above (Sec. 2.1) there are three rain events on that day, early morning around 03 UTC, between 09 and 13 UTC and around 20 UTC Fig. 2 (a). One can see that during all rain events with rain rates between 0 and at maximum  $10 \text{ mm h}^{-1}$  the spectral consistency check failed (Fig. 2 b). The presence of the rain in the lower atmosphere or even accumulated liquid water on the radome compromises the retrieval output indicated by the unrealistic spikes in the temperature profiles (b, d, f) and by a high temperature difference (c, e, g). It is obvious that neither the  $4\nu z10\varphi$  nor the  $4\nu10\varphi$  nor the  $7\nu9\varphi$  work during rain conditions. However, the  $4\nu9\varphi$  retrieval can tackle the rain limitation and is able to produce reasonable results in comparison to the ECMWF model temperature output (h, i) with the lowest temperature differences during rainy periods.

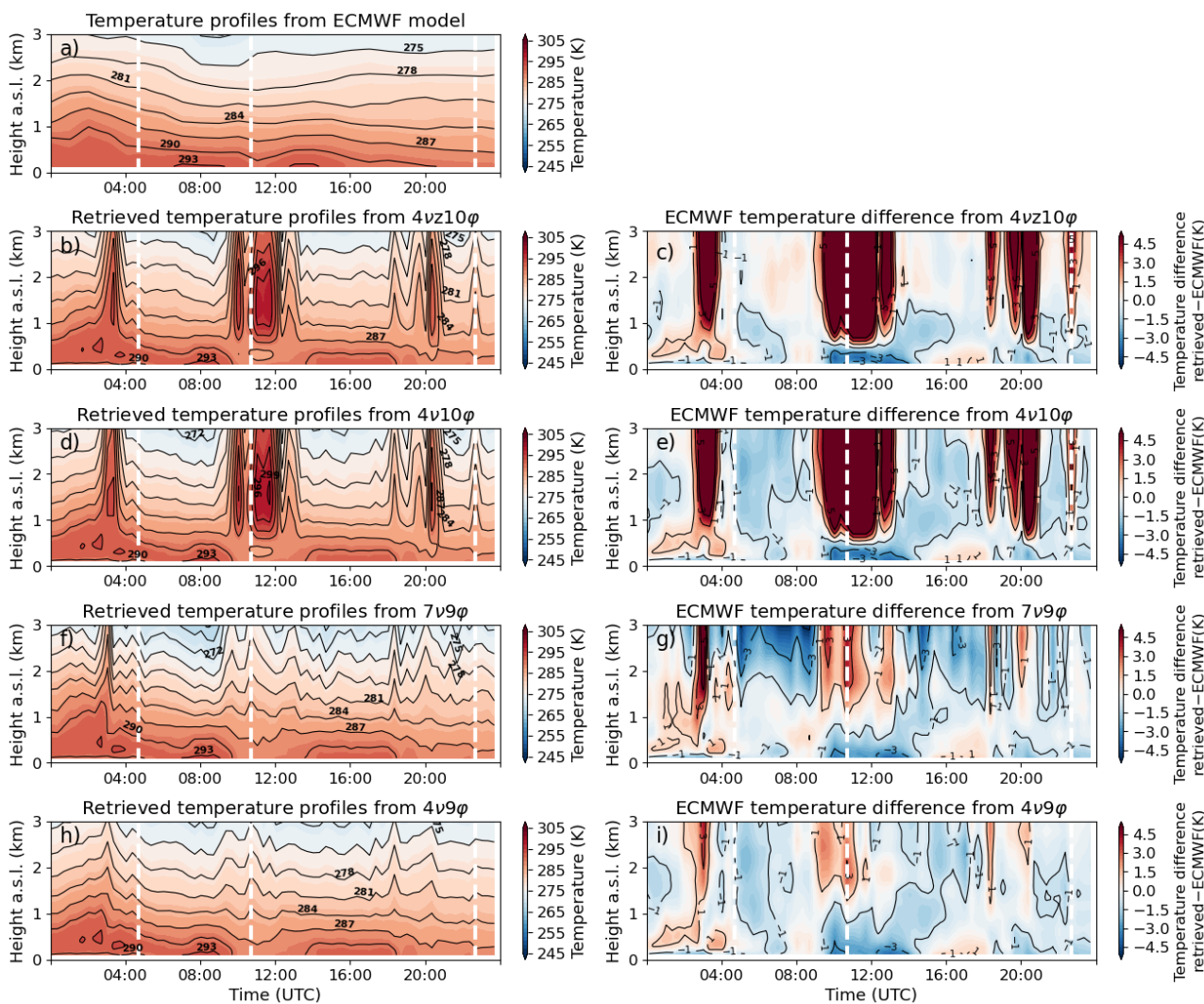


**Figure 6.** Height-time series of temperature profiles from ECMWF model (a) and temperature profiles based on different retrieval algorithms (b, d, f, h) and associated temperature difference to ECMWF model (c, e, g, i) in Lindenberg (Germany) on Aug 26, 2020. The radiosonde launch times are indicated by white dashed lines.

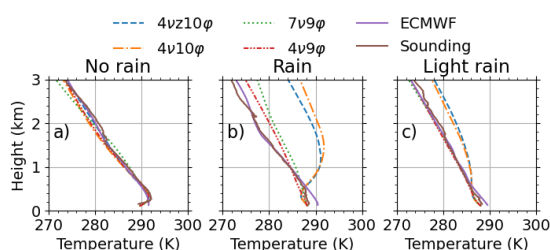


Figure 7 illustrates a comparison between the retrieved temperature profiles and three radiosonde launches at MOL-RAO on Aug 26, 2020, 04:45 (a), 10:45 (b) and 22:25 UTC (c). During the launch at 04:45 UTC in non-raining conditions there are no significant differences between the retrievals, the sounding and the ECMWF temperature profiles (a). The differences are much higher during the rain event at 10:45 UTC (b). Sounding and ECMWF model temperature profile are in good agreement and only the  $7\nu9\varphi$  and the  $4\nu9\varphi$  retrievals fit the sounding as reference within less than 2 K near the surface and 4 K and 3 K, respectively, at 2 km. In contrast, the temperature retrievals from  $4\nu z10\varphi$  and  $7\nu z10\varphi$ , are completely off by over 10 K above 1 km. The temperature profile comparison during short and light rain event at around 22:45 UTC in Fig. 7c) shows a similar result, the  $7\nu9\varphi$  and the  $4\nu9\varphi$  retrieval even fit to the reference sounding within the expected sounding uncertainty.

Up to this point, the performance of the retrieval has been evaluated only on the basis of case studies. In the next section it will be evaluated against ECMWF model using a larger data set.

### 4.3 ECMWF model comparison

In this section the performance of the proposed  $4\nu9\varphi$  and the state-of-the-art  $4\nu z10\varphi$  temperature retrieval against ECMWF model temperature profiles is investigated. Therefore, all three months of HATPRO observation at MOL-RAO from July to October 2020 are taken into account. Hourly ECMWF model temperatures are interpolated to the measurement grid of approximately 20 minutes per temperature profile. Figure 8 shows the retrieval performance in terms of bias (left panels) and standard deviation (right panels) between ECMWF output and retrievals for non-raining cases (a, b), and raining cases with rain rates smaller than  $0.5\text{ mm h}^{-1}$  (c, d), rain rates between  $0.5$  and  $2\text{ mm h}^{-1}$  (e, f) and rain rates larger than  $2\text{ mm h}^{-1}$  (g, h). During non-raining conditions (3732 sample profiles) both retrievals agree well with the ECMWF output (Fig. 8 a, b) as could be expected from Fig. 5. But for small rain rates (61 sample profiles) the proposed  $4\nu9\varphi$  agrees much better with a bias less than 1 K (Fig. 8 c) and a standard deviation ranging between 0.5 and 2 K (d). The state-of-the-art retrieval ( $4\nu z10\varphi$ ) leads to very high deviations from the ECMWF temperature profiles with biases and standard deviations around 5 to 7 K apart from altitudes above 0.5 km. The higher the rain rate, the worse the performance of the MWR temperature profile retrievals. Although the  $4\nu9\varphi$  is significantly better than the common  $4\nu z10\varphi$  retrieval, it deviates from the ECMWF output by 6 K (bias) at 3 km altitude in heavy rain. Of course the ECMWF model output is not the truth, especially in rain, but serves as a



**Figure 7.** Panels a, b, and c show a comparison of three retrieved temperature profiles with radio-soundings launched at MOL-RAO on Aug 26, 2020, at 4:45 (a), 10:45 (b), and 22:45 UTC (c) and ECMWF model output from 5, 11, and 23 UTC.

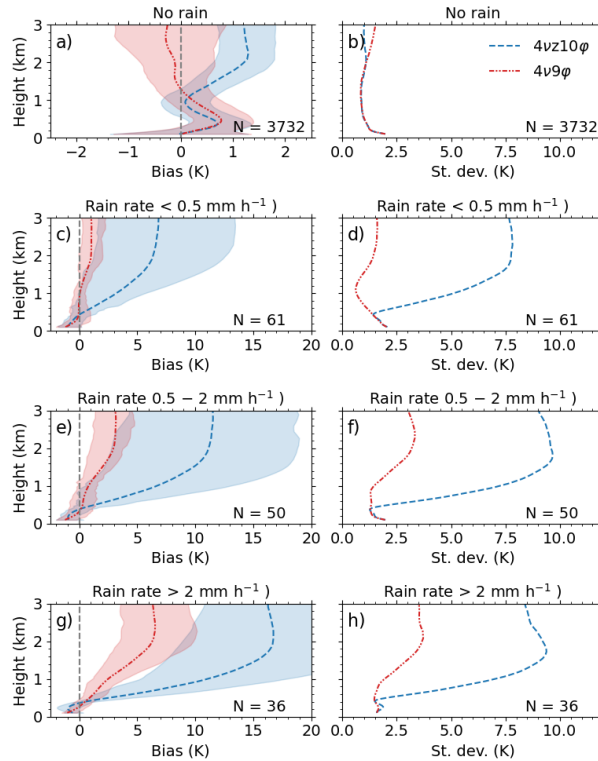


**Figure 8.** Bias (left panel) and standard deviation (right panel) between retrieved and ECMWF temperature profiles for rainfree cases (a, b), and raining cases with rain rates smaller than  $0.5 \text{ mm h}^{-1}$  (c, d), rain rates between  $0.5$  and  $2 \text{ mm h}^{-1}$  (e, f) and rain rates larger than  $2 \text{ mm h}^{-1}$  (g, h). Red lines (dash dot dot) mark the  $4\nu 9\phi$  retrieval and blue dashed lines mark the common  $4\nu z10\phi$  retrieval. N denotes the number of time steps taken into account at MOL-RAO between 16 Jul, 2020 and 8 Oct, 2020. Bias is defined as retrieved minus ECMWF output as reference. The colored area marks values between the 25 and 75 percentile. Note that in (a) the x-axis is different from that in the other panels.

275 reference for comparing the two retrievals. It should be noted that the new  $4\nu 9\phi$  retrieval performs better since the common  $4\nu z10\phi$  retrieval setup was intentionally not developed for working under raining conditions. Summarizing, that the new proposed retrieval based on MWR observation under lower elevation angles and only the higher V-band frequencies allows to resolve temperature profiles during rain with rain rates up to  $2 \text{ mm h}^{-1}$  which was not possible before with the state-of-the-art retrievals.

## 280 5 Conclusions and Outlook

In summary, the HATPRO  $4\nu 9\phi$  retrieval method demonstrated in this study achieves unprecedented accuracy of low-level temperature profiling up to 2 km in rain. It was shown that even in heavier rain measurements at elevation angles below  $40^\circ$



can be used to derive temperature profiles up to 1.5 km. The temperature retrievals can be easily applied with an existing open source software (mwrpy). In addition, the published software package can be used to create custom retrievals for arbitrary locations (Foth, 2023a). This represents a significant improvement towards the reliability of using MWR for weather nowcasting or forecast. Especially investigations of evaporative cooling during precipitation evaporation are often very inaccurate due to incorrect assumptions of temperature which can compromise the reliability of the evaluation of model parameterizations. Furthermore, the proposed method can be applied retrospectively to correct temperature profiles from long-term observations as long as the MWR scanning brightness temperature data is available for the post-processing.

290

In the future, an optimal estimation method which is also a variational technique should be used in further investigations. In contrast to Cimini et al. (2011), only HATPRO frequencies that pass the consistency check for all elevation angles should be used at each time step independent of the rain situation. Thus, a continuous time series of temperature profiles can be created, which provides physical uncertainties for each time and height range. This might also improve profiles of absolute humidity which is also of interest for the evaporation studies. Additionally, long-term HATPRO observations will enable a quantification of the maximum rain rate at which the new  $4\nu_{9\varphi}$  retrieval can be applied.

295

*Code and data availability.* The HATPRO raw data is processed with mwrpy version 4.3.0 (<https://github.com/actris-cloudnet/mwrpy>). Also some mwrpy subroutines for plotting are used in this study. The optimal estimation software package pyOptimalEstimation version 1.2 is available under <https://github.com/maahn/pyOptimalEstimation> and described in detail in Maahn et al. (2020). The Passive and Active Microwave TRANSfer model PAMTRA is also available on github.com (<https://github.com/igmk/pamtra>) and is already published in Mech et al. (2019, 2020). ERA5 data is available under <https://cds.climate.copernicus.eu/> (Hersbach et al., 2019). The HATPRO data from the general scans in Leipzig is available at zenodo (Foth, 2023b). The Lindenberg HATPRO and model data used in this study are generated by the Aerosol, Clouds and Trace Gases Research Infrastructure (ACTRIS) and are available from the ACTRIS Data Centre using the following links: <https://doi.org/10.60656/ca8017ee6ef94027>, <https://doi.org/10.60656/E938967BC0524DEE>. The retrievals are made with the pyMakeRetrieval routines (Foth, 2023a) and are available on github (<https://github.com/remsens-lim/pyMakeRetrieval>).

300

305

*Author contributions.* AF prepared the manuscript in close cooperation with ML, PSG and HKL. AF performed the investigations and data analyses. ML and AF realized the experimental setup in Lindenberg and Leipzig, respectively, and were responsible for the high quality of the HATPRO measurements. The conceptualization was initialized by AF, ML and PSG. All authors have contributed to the scientific discussions.

310 *Competing interests.* The authors declare that they have no conflict of interest.



*Acknowledgements.* The authors thank the LIM-team and the MOL-RAO team for supporting the HATPRO observations in Lindenberg. The authors also acknowledge the ACTRIS-Cloudnet team and all associated developers for the well documented code around remote sensing especially the HATPRO processing within mwrpy. This research has been supported by the German Science Foundation (DFG) (grant nos. FO 1285/2-11). PSG was funded by the Deutsche Forschungsgemeinschaft (DFG), Transregio-project TR-172 Arctic Amplification (AC)<sup>3</sup> 315 (grant 268020496), sub-project B07 (grant 437153667). This research has been supported by the Federal State of Saxony and the European Social Fund (ESF) in the framework of the program “Projects in the fields of higher education and research” (grant no. 232101734 and 100339509).





## References

- Araki, K., Murakami, M., Ishimoto, H., and Tajiri, T.: Ground-Based Microwave Radiometer Variational Analysis during No-Rain and Rain  
320 Conditions, *Sola*, 11, 108–112, <https://doi.org/10.2151/sola.2015-026>, 2015.
- Cimini, D., Campos, E., Ware, R., Albers, S., Giuliani, G., Oreamuno, J., Joe, P., Koch, S. E., Cober, S., and Westwater, E.: Thermodynamic  
Atmospheric Profiling During the 2010 Winter Olympics Using Ground-Based Microwave Radiometry, *IEEE Trans. Geosci. Remote  
Sens.*, 49, 4959–4969, <https://doi.org/10.1109/TGRS.2011.2154337>, 2011.
- Cimini, D., Rosenkranz, P. W., Tretyakov, M. Y., Koshelev, M. A., and Romano, F.: Uncertainty of Atmospheric Microwave Ab-  
325 sorption Model: Impact on Ground-Based Radiometer Simulations and Retrievals, *Atmospheric Chem. Phys.*, 18, 15 231–15 259,  
<https://doi.org/10.5194/acp-18-15231-2018>, 2018.
- Crewell, S. and Löhnert, U.: Accuracy of Boundary Layer Temperature Profiles Retrieved With Multifrequency Multiangle Microwave  
Radiometry, *IEEE Trans. Geosci. Remote Sensing*, 45, 2195–2201, <https://doi.org/10.1109/TGRS.2006.888434>, 2007.
- Decker, M. T., Westwater, E. R., and Guiraud, F. O.: Experimental Evaluation of Ground-Based Microwave Radiometric Sensing  
330 of Atmospheric Temperature and Water Vapor Profiles, *J. Appl. Meteorol. Climatol.*, 17, 1788–1795, [https://doi.org/10.1175/1520-0450\(1978\)017<1788:EEOGBM>2.0.CO;2](https://doi.org/10.1175/1520-0450(1978)017<1788:EEOGBM>2.0.CO;2), 1978.
- Fehlmann, M., Rohrer, M., von Lerber, A., and Stoffel, M.: Automated Precipitation Monitoring with the Thies Disdrometer: Biases and  
Ways for Improvement, *Atmospheric Meas. Tech.*, 13, 4683–4698, <https://doi.org/10.5194/amt-13-4683-2020>, 2020.
- Foth, A.: pyMakeRetrieval v1.1.1, Zenodo, <https://doi.org/10.5281/ZENODO.10014291>, 2023a.
- 335 Foth, A.: Brightness Temperature Data and Weather Station Data from General Scans of the Microwave Radiometer HATPRO, 2023b.
- Foth, A. and Pospichal, B.: Optimal Estimation of Water Vapour Profiles Using a Combination of Raman Lidar and Microwave Radiometer,  
*Atmos. Meas. Tech.*, 10, 3325–3344, <https://doi.org/10.5194/amt-10-3325-2017>, 2017.
- Güldner, J. and Spänkuch, D.: Results of Year-Round Remotely Sensed Integrated Water Vapor by Ground-Based Microwave Radiometry, *J  
Appl Meteor Clim.*, 38, 981–988, [https://doi.org/10.1175/1520-0450\(1999\)038<0981:ROYRRS>2.0.CO;2](https://doi.org/10.1175/1520-0450(1999)038<0981:ROYRRS>2.0.CO;2), 1999.
- 340 Hersbach, H., Bell, B., Berrisford, P., Biavati, G., Horányi, A., Muñoz Sabater, J., Nicolas, J., Peubey, C., Radu, R., Rozum, I.,  
Schepers, D., Simmons, A., Soci, C., Dee, D., and Thépaut, J.-N.: ERA5 Hourly Data on Pressure Levels from 1940 to Present,  
<https://doi.org/10.24381/cds.6860a573>, 2019.
- Illingworth, A. J., Hogan, R. J., O'Connor, E., Bouniol, D., Brooks, M. E., Delanoé, J., Donovan, D. P., Eastment, J. D., Gaussiat, N., Goddard,  
J. W. F., Haefelin, M., Baltink, H. K., Krasnov, O. A., Pelon, J., Piriou, J.-M., Protat, A., Russchenberg, H. W. J., Seifert, A., Tompkins,  
345 A. M., van Zadelhoff, G.-J., Vinit, F., Willén, U., Wilson, D. R., and Wrench, C. L.: Cloudnet: Continuous Evaluation of Cloud Profiles in  
Seven Operational Models Using Ground-Based Observations, *B. Am. Meteorol. Soc.*, 88, 883–898, <https://doi.org/10.1175/BAMS-88-6-883>, 2007.
- Jensen, M. P., Holdridge, D. J., Survo, P., Lehtinen, R., Baxter, S., Toto, T., and Johnson, K. L.: Comparison of Vaisala Radiosondes RS41  
and RS92 at the ARM Southern Great Plains Site, *Atmospheric Meas. Tech.*, 9, 3115–3129, <https://doi.org/10.5194/amt-9-3115-2016>,  
350 2016.
- Karstens, U., Simmer, C., and Ruprecht, E.: Remote Sensing of Cloud Liquid Water, *Meteorol. Atmos. Phys.*, 54, 157–171,  
<https://doi.org/10.1007/BF01030057>, 1994.
- Kazama, S., Rose, T., Zimmermann, R., and Zimmermann, R.: A Precision Autocalibrating 7 Channel Radiometer for Environmental Re-  
search Applications, *J. Remote Sens. Soc. Jpn.*, 19, 265–273, <https://doi.org/10.11440/rssj1981.19.265>, 1999.



- 355 Kuchler, N., Turner, D. D., Löhnert, U., and Crewell, S.: Calibrating Ground-based Microwave Radiometers: Uncertainty and Drifts, *Radio Sci.*, 51, 311–327, <https://doi.org/10.1002/2015RS005826>, 2016.
- Liebe, H. J., Hufford, G. A., and Cotton, M. G.: Propagation Modeling of Moist Air and Suspended Water/Ice Particles at Frequencies below 1000 GHz, AGARD, 1993.
- Löhnert, U. and Crewell, S.: Accuracy of Cloud Liquid Water Path from Ground-Based Microwave Radiometry 1. Dependency on Cloud  
360 Model Statistics, *Radio Sci.*, 38, 8041, <https://doi.org/10.1029/2002RS002654>, 2003.
- Löhnert, U. and Maier, O.: Operational Profiling of Temperature Using Ground-Based Microwave Radiometry at Payerne: Prospects and Challenges, *Atmos. Meas. Tech.*, 5, 1121–1134, <https://doi.org/10.5194/amt-5-1121-2012>, 2012.
- Löhnert, U., van Meijgaard, E., Baltink, H. K., Groß, S., and Boers, R.: Accuracy Assessment of an Integrated Profiling Technique for Operationally Deriving Profiles of Temperature, Humidity, and Cloud Liquid Water, *J. Geophys. Res.*, 112, D04205,  
365 <https://doi.org/10.1029/2006JD007379>, 2007.
- Maahn, M., Turner, D. D., Löhnert, U., Posselt, D. J., Ebell, K., Mace, G. G., and Comstock, J. M.: Optimal Estimation Retrievals and Their Uncertainties: What Every Atmospheric Scientist Should Know, *Bull. Amer. Meteor. Soc.*, <https://doi.org/10.1175/BAMS-D-19-0027.1>, 2020.
- Maschwitz, G., Löhnert, U., Crewell, S., Rose, T., and Turner, D. D.: Investigation of Ground-Based Microwave Radiometer Calibration  
370 Techniques at 530 hPa, *Atmos. Meas. Tech.*, 6, 2641–2658, <https://doi.org/10.5194/amt-6-2641-2013>, 2013.
- Mech, M., Maahn, M., Ori, D., and Orlandi, E.: PAMTRA: Passive and Active Microwave TRANSfer Tool v1.0, Zenodo, <https://doi.org/10.5281/zenodo.3582992>, 2019.
- Mech, M., Maahn, M., Kneifel, S., Ori, D., Orlandi, E., Kollias, P., Schemann, V., and Crewell, S.: PAMTRA 1.0: The Passive and Active Microwave Radiative TRANSfer Tool for Simulating Radiometer and Radar Measurements of the Cloudy Atmosphere, *Geosci. Model  
375 Dev.*, 13, 4229–4251, <https://doi.org/10.5194/gmd-13-4229-2020>, 2020.
- Nash, J., Smout, R., Oakley, T., Pathack, B., and Kurnosenko, S.: WMO Intercomparison of High Quality Radiosonde Systems: Final Report, WMO Rep., p. 118 pp, 2005.
- Rodgers, C. D.: *Inverse Methods for Atmospheric Sounding - Theory and Practice*, vol. 2, World Scientific Publishing, 2000.
- Rose, T., Crewell, S., Löhnert, U., and Simmer, C.: A Network Suitable Microwave Radiometer for Operational Monitoring of the Cloudy  
380 Atmosphere, *Atmos. Res.*, 75, 183–200, <https://doi.org/10.1016/j.atmosres.2004.12.005>, 2005.
- Rosenkranz, P. W.: Water Vapor Microwave Continuum Absorption: A Comparison of Measurements and Models, *Radio Sci.*, 33, 919–928, <https://doi.org/10.1029/98RS01182>, 1998.
- Schnitt, S., Foth, A., Kalesse-Los, H., Mech, M., Acquistapace, C., Jansen, F., Löhnert, U., Pospichal, B., Röttenbacher, J., Crewell, S., and Stevens, B.: Ground- and Ship-Based Microwave Radiometer Measurements during EUREC<sup>4</sup>A, *Earth Syst. Sci. Data*, 16, 681–700,  
385 <https://doi.org/10.5194/essd-16-681-2024>, 2024.
- Simmer, C.: *Satellitenfernerkundung Hydrologischer Parameter Der Atmosphäre Mit Mikrowellen*, Kovač, 1994.
- Solheim, F., Godwin, J. R., Westwater, E. R., Han, Y., Keihm, S. J., Marsh, K., and Ware, R.: Radiometric Profiling of Temperature, Water Vapor and Cloud Liquid Water Using Various Inversion Methods, *Radio Sci.*, 33, 393–404, <https://doi.org/10.1029/97RS03656>, 1998.
- Sun, B., Reale, T., Schroeder, S., Pettey, M., and Smith, R.: On the Accuracy of Vaisala RS41 versus RS92 Upper-Air Temperature Observa-  
390 tions, *J. Atmospheric Ocean. Technol.*, 36, 635–653, <https://doi.org/10.1175/JTECH-D-18-0081.1>, 2019.



- Turner, D., Cadetdu, M., Löhnert, U., Crewell, S., and Vogelmann, A.: Modifications to the Water Vapor Continuum in the Microwave Suggested by Ground-Based 150-GHz Observations, *IEEE Trans. Geosci. Remote Sensing*, 47, 3326–3337, <https://doi.org/10.1109/TGRS.2009.2022262>, 2009.
- Turner, D. D., Lesht, B. M., Clough, S. A., Liljegren, J. C., Revercomb, H. E., and Tobin, D. C.: Dry Bias and Variability in Vaisala RS80-H Radiosondes: The ARM Experience, *J. ATMOSPHERIC Ocean. Technol.*, 20, 16, 2003.
- Walbröl, A., Crewell, S., Engelmann, R., Orlandi, E., Griesche, H., Radenz, M., Hofer, J., Althausen, D., Maturilli, M., and Ebell, K.: Atmospheric Temperature, Water Vapour and Liquid Water Path from Two Microwave Radiometers during MOSAiC, *Sci Data*, 9, 534, <https://doi.org/10.1038/s41597-022-01504-1>, 2022.
- Wandinger, U.: Raman Lidar, in: *Lidar – Range-Resolved Optical Remote Sensing of the Atmosphere*, edited by Weitkamp, C., vol. 102 of *Springer Series in Optical Sciences*, pp. 241–271, Springer Berlin/Heidelberg, 2005.
- Ware, R., Cimini, D., Herzegh, P., Marzano, F., Vivekanandan, J., and Westwater, E.: Ground-Based Microwave Radiometer Measurements during Precipitation, in: *8th Specialist Meeting on Microwave Radiometry*, p. 3, Rome, Italy, 2004.
- Ware, R., Cimini, D., Campos, E., Giuliani, G., Albers, S., Nelson, M., Koch, S. E., Joe, P., and Cober, S.: Thermodynamic and Liquid Profiling during the 2010 Winter Olympics, *Atmospheric Research*, 132–133, 278–290, <https://doi.org/10.1016/j.atmosres.2013.05.019>, 2013.
- Westwater, E. R., Crewell, S., Mätzler, C., and Cimini, D.: Principles of Surface-Based Microwave and Millimeter Wave Radiometric Remote Sensing of the Troposphere, *Quad. Soc. Ital. Elettromagnetismo*, 1, 50–90, 2005.
- Xu, G., Ware, R. S., Zhang, W., Feng, G., Liao, K., and Liu, Y.: Effect of Off-Zenith Observations on Reducing the Impact of Precipitation on Ground-Based Microwave Radiometer Measurement Accuracy, *Atmospheric Research*, 140–141, 85–94, <https://doi.org/10.1016/j.atmosres.2014.01.021>, 2014.